Mutual synergy between catalase and peroxidase activities of the bifunctional enzyme KatG is facilitated by electron hole-hopping within the enzyme

Received for publication, April 18, 2017, and in revised form, September 22, 2017 Published, Papers in Press, September 27, 2017, DOI 10.1074/jbc.M117.791202

Olive J. Njuma[‡1], Ian Davis[§¶], Elizabeth N. Ndontsa[‡2], Jessica R. Krewall[‡], Aimin Liu[§], and Douglas C. Goodwin[‡3]

From the [‡]Department of Chemistry and Biochemistry, Auburn University, Auburn, Alabama 36849-5312, the [§]Department of Chemistry, University of Texas at San Antonio, San Antonio, Texas 78249-0698, and the [¶]Department of Chemistry, Georgia State University, Atlanta, Georgia 30303

Edited by Ruma Banerjee

KatG is a bifunctional, heme-dependent enzyme in the front-line defense of numerous bacterial and fungal pathogens against H_2O_2-induced oxidative damage from host immune responses. Contrary to the expectation that catalase and peroxidase activities should be mutually antagonistic, peroxidatic electron donors (PxEDs) enhance KatG catalase activity. Here, we establish the mechanism of synergistic cooperation between these activities. We show that at low pH values KatG can fully convert H_2O_2 to O_2 and H_2O only if a PxED is present in the reaction mixture. Stopped-flow spectroscopy results indicated rapid initial rates of H_2O_2 disproportionation slowing concomitantly with the accumulation of ferryl-like heme states. These states very slowly returned to resting (*i.e.* ferric) enzyme, indicating that they represented catalase-inactive intermediates. We also show that an active-site tryptophan, Trp-321, participates in off-pathway electron transfer. A W321F variant in which the proximal tryptophan was replaced with a non-oxidizable phenylalanine exhibited higher catalase activity and less accumulation of off-pathway heme intermediates. Finally, rapid freeze-quench EPR experiments indicated that both WT and W321F KatG produce the same methionine–tyrosine–tryptophan (MYW) cofactor radical intermediate at the earliest reaction time points and that Trp-321 is the preferred site of off-catalase protein oxidation in the native enzyme. Of note, PxEDs did not affect the formation of the MYW cofactor radical but could reduce nonproductive protein-based radical species that accumulate during reaction with H_2O_2. Our results suggest that catalase-inactive intermediates accumulate because of off-mechanism oxidation, primarily of Trp-321, and PxEDs stimulate KatG catalase activity by preventing the accumulation of inactive intermediates.

Catalase-peroxidase (KatG)[4] is a bifunctional heme-dependent enzyme found in bacteria and lower eukaryotes (1), which is integral to the defense of these organisms against H_2O_2 toxicity (2, 3). KatG function appears to carry especially important ramifications for plant and animal pathogens (4–6) because these organisms are likely to encounter excess H_2O_2 produced by their host's immune response (*e.g.* oxidative burst). Among these enzymes, the function of KatG in *Mycobacterium tuberculosis* (*Mt*KatG) is especially important because it is the only catalase-active enzyme carried by *M. tuberculosis* (7), and it activates the front-line antitubercular agent isoniazid (INH) (8). KatG-dependent oxidation of INH initiates formation of isonicotinyl-NAD, which inhibits an enoyl reductase (InhA) essential for mycolic acid biosynthesis (9). Accordingly, a large proportion of INH-resistant *M. tuberculosis* strains (>50%) produce an altered KatG (*e.g.* S315T) incapable of activating the drug (10, 11), rendering ineffective one of the most widely available and inexpensive antitubercular agents. The precise mechanism by which KatG activates INH and the molecular basis for how mutations to the *katG* gene interfere in said activation are the subjects of ongoing investigations (12–15).

KatG catalyzes H_2O_2 disproportionation to produce H_2O and O_2 (*i.e.* it is a catalase). It does so with an apparent second-order rate constant ($\sim 1 \times 10^6$ M^{-1} s^{-1}) similar to typical (*i.e.* monofunctional) catalases (16, 17) even though it shares no structural homology with them. Instead, it is a member of the plant peroxidase-like superfamily with cytochrome *c* peroxidase (C*c*P), ascorbate peroxidase (APx), and horseradish peroxidase (HRP) (18, 19). Indeed, the active sites of C*c*P, APx, and KatG are virtually superimposable (Fig. 1) (20–24). Not surprisingly, then, KatG also catalyzes H_2O_2 reduction to H_2O concomitant with the oxidation of a structurally diverse range of exogenous electron donors (*i.e.* it is a peroxidase). Its peroxidase activity is well within the range of other plant peroxidase-like superfamily members (16, 17, 25), but KatG is the only member of the entire superfamily that possesses appreciable catalase activity.

This work was supported in part by Grants MCB 1616059 and MCB 0641614 from the National Science Foundation (to D. C. G.) and National Institutes of Health Grant GM108988 (to A. L.). The authors declare that they have no conflicts of interest with the contents of this article. The content is solely the responsibility of the authors and does not necessarily represent the official views of the National Institutes of Health.

[1] Present address: Dept. of Biochemistry, Vanderbilt University School of Medicine, Nashville, TN 37232-0146.

[2] Present address: Aduro Biotech, Inc., 740 Heinz Ave., Berkeley, CA 94710-2224.

[3] To whom correspondence should be addressed: Dept. of Chemistry and Biochemistry, 179 Chemistry Bldg., Auburn University, Auburn, AL 36849-5312. Tel.: 334-844-6992; Fax: 334-844-6959; E-mail: goodwdc@auburn.edu.

[4] The abbreviations used are: KatG, catalase-peroxidase; *Mt*KatG, *M. tuberculosis* KatG; MYW, methionine–tyrosine–tryptophan covalent adduct; C*c*P, cytochrome *c* peroxidase; APx, ascorbate peroxidase; LL1, large loop 1; LL2, large loop 2; ABTS, 2,2′-azino-bis(3-ethylbenzthiazoline-6-sulfonate); INH, isoniazid; PxED, peroxidatic electron donor; PAA, peracetic acid; μW, microwatt.

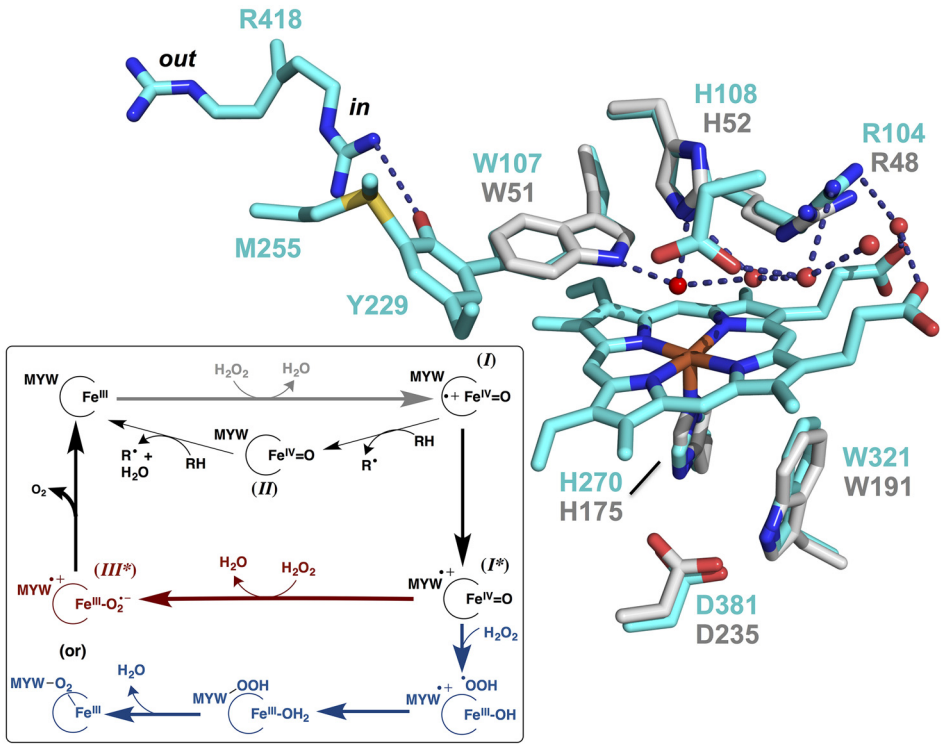

Figure 1. Superposition of KatG and CcP active sites as well as a putative superposition of the catalase and peroxidase catalytic cycles of KatG. KatG is shown with carbons in *cyan*, and CcP is shown with carbons in *gray*. The active-site waters (*red spheres*) and heme are from KatG, and the two conformations (*in* and *out*) of the arginine switch (*R418*) are shown. KatG numbering is according to the *M. tuberculosis* enzyme *Mt*KatG. This image was generated using MacPyMOL 1.6.0.0 (77) using coordinates from Protein Data Bank code 2CCA (78) and 2CYP (24) for *Mt*KatG and yeast CcP, respectively. Putatitve superposition of the catalase and peroxidase cycles of KatG is shown in the *inset*. The reaction common to both (compound I formation) is shown with the *bold gray arrow*. Additional steps of classical peroxidase activity are shown with *thin arrows*. The additional steps of catalase activity are shown in *bold arrows*, including two proposed mechanisms (*red versus blue*) for the return of compound I* to the starting state.

Despite their striking active-site similarities, KatG possesses structural features that distinguish it from other members of its superfamily. Among them are two large loops (LL1 and LL2), both of which are essential for KatG function (20–22, 26, 27). Both loops also contribute to a much narrower channel to the active-site heme, which among other things restricts access of many peroxidatic electron donors (PxEDs) to the heme edge (22, 27–29). Additionally, LL1 bears an invariant tyrosine (Tyr-229 by *Mt*KatG numbering) that participates in a unique methionine–tyrosine–tryptophan (MYW) adduct that serves as a protein-derived cofactor (20–22, 30, 31). Substitutions of any of the residues of the MYW adduct consistently produce KatG variants that retain or increase their peroxidase activity but have negligible catalase activity (14, 29, 32–37).

Commensurate with an active site completely distinct from typical catalases, it is clear that KatG operates by a novel catalase mechanism, although the details remain a matter of debate (15, 38–47). The first step is common to all heme-dependent catalases and peroxidases and is widely agreed upon for KatG; H_2O_2 oxidizes the ferric heme of KatG to form a ferryl-oxo porphyrin π cation radical ($Fe^{IV}=O[porphyrin^{+\cdot}]$) known as compound I (Fig. 1, *inset*). At this point, KatG diverges from the canonical catalase mechanism by reducing the porphyrin radical via an intramolecular electron transfer from the MYW adduct, generating the KatG-unique compound I* (*i.e.* $Fe^{IV}=O[MYW]^{+\cdot}$). Two paths have been proposed for the subsequent reaction of compound I* with H_2O_2 and return to the resting state. One posits formation of a ferric-superoxide complex known in peroxidase vernacular as compound III. Because of the presence of the MYW radical, this is referred to as compound III* (*i.e.* $Fe^{III}–O_2^{-}[MYW]^{+\cdot}$). Intramolecular electron transfer from the $Fe^{III}–O_2^{-}$ heme to the MYW radical is proposed to return the enzyme to its ferric state along with the release of O_2 (38–40). Alternatively, others have proposed that H_2O_2 is oxidized to the peroxyl radical by the $Fe^{IV}=O$ heme center of compound I*. Deprotonation of the indole of the MYW radical then permits formation of an MYW perhydroxy–indole intermediate followed by a bridged $Fe^{III}–O_2$-MYW complex, which then decomposes to release O_2 and return to the starting state (44).

The arginine switch is invariant among KatGs (Arg-418 in *Mt*KatG), and its conformation is pH-dependent (48–52). Structures solved for a bacterial KatG at pH 8.5 show the guanidinium moiety of the switch forms a salt bridge with the tyrosyl phenoxide anion of the MYW cofactor (*in* Fig. 1). At pH 4.5, the arginine side chain is oriented away from the MYW adduct and toward the surface of KatG (*out* Fig. 1). At pH 6.5, corresponding roughly to the optimum pH for catalase activity, this arginine equally populates both conformational states (48, 49). Substitution of Arg-418 with Leu, Ala, or Asn, but not Lys, sharply diminishes the catalase activity of KatG (39, 49, 50, 52), and as has been recently shown with *Magnaporthe grisea* extracellular KatG, it eliminates the pH dependence of catalase activity (52). The mechanism by which Arg-418 facilitates catalatic turnover is still under investigation. In general, its occupation of the out conformation is connected with MYW oxida-

tion, whereas the in conformation is connected with reduction of the MYW radical (39, 44, 45, 49, 53). Interestingly, a recent computational study suggests that Arg-418 facilitates the rotation of the Tyr and Trp aromatic rings with respect to one another, helping enable reduction of the MYW radical by the $Fe^{III}–O_2^{\cdot-}$ heme (45).

What then is the place of peroxidase activity and PxEDs in KatG catalysis? As both catalase and peroxidase catalytic mechanisms involve the H_2O_2-dependent formation of compound I, the only difference between the two activities is the route by which the enzyme returns to the ferric state. As outlined above, catalase turnover requires the oxidation of a second H_2O_2; however, with peroxidases an exogenous (usually aromatic) electron donor is oxidized instead. Typically, compound I is reduced by one electron to produce compound II ($Fe^{IV}=O$) and the corresponding PxED radical (Fig. 1, *inset*). A second single-electron transfer returns the enzyme to the ferric state and produces a second equivalent of the PxED radical. According to this model, one would anticipate that peroxidase and catalase activities should be mutually antagonistic, and in particular, PxEDs should inhibit catalase activity. Indeed, the first published report on a catalase-peroxidase showed that the classical peroxidase electron donor *o*-dianisidine did inhibit catalase activity at pH 7 (54). However, we have recently shown that a number of PxEDs can stimulate the catalase activity of KatG by over an order of magnitude (55). Interestingly, this synergistic effect is most prominent at lower pH (*i.e.* ~pH 5) and ~1 mM H_2O_2, conditions that coincide with antimicrobial defenses like the neutrophil-based oxidative burst. Clearly, the inter-relationship between the catalatic and peroxidatic mechanisms of KatG is more complex than has been previously appreciated.

In this report, we investigate the mechanism by which PxEDs stimulate the catalase activity of KatG. At low pH and in the absence of a PxED, O_2 production ceases well short of the expected catalase stoichiometry, and only the addition of more enzyme is able to restart O_2 generation. There is also a substantial lag between the conclusion of H_2O_2 consumption and the return of the enzyme to its ferric state, which suggests that catalase-inactive intermediates accumulate during multiple turnovers. Proposed KatG catalase mechanisms require precise intramolecular electron transfer from the MYW cofactor (44, 45). We surmised that inactivation may occur due to off-catalase electron transfer, a problem that could be resolved by inclusion of a PxED. Furthermore, because the enzyme's proximal tryptophan (*W321,* Fig. 1) has shown a propensity (observed experimentally and computationally) toward oxidation to form a radical intermediate (53, 56–59), we also surmised that the proximal Trp is a likely participant in off-pathway electron transfers leading to catalase-inactive intermediates. To test these hypotheses, we replaced the proximal tryptophan with non-oxidizable phenylalanine (W321F KatG) and compared it with wild-type KatG (*wt*KatG). Optical stopped-flow, rapid freeze-quench EPR, and steady-state kinetic analyses of both proteins were carried out in the presence and absence of PxEDs. Our results suggest that catalase-inactive intermediates accumulate due to off-mechanism oxidation, primarily of Trp-321, and PxEDs stimulate KatG catalase activity by preventing the accumulation of inactive intermediates. This informs a new model wherein the synergistic interplay of the two most dominant activities of KatG is facilitated by electron hole-hopping from the active site to the KatG surface via Trp-321.

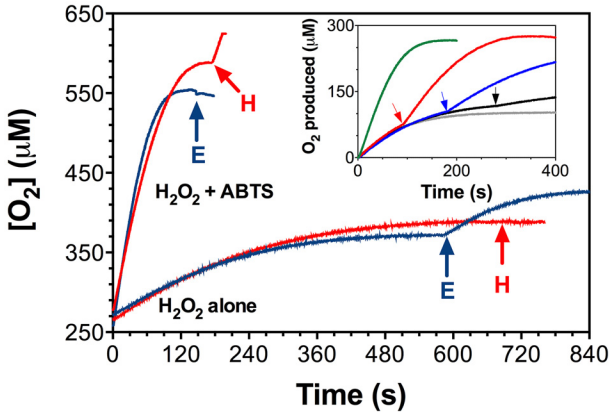

Figure 2. Effect of ABTS (a PxED) on the rate and amount of catalatic O_2 production by KatG. All reactions contained 5 nM KatG in 50 mM acetate, pH 5.0, and were initiated by the addition of 0.5 mM H_2O_2. When present, ABTS was included at 0.1 mM, and all reactions were carried out at 23 °C. In the *main graph*, second additions of H_2O_2 (0.5 mM) or KatG (5.0 nM) are indicated by *H* and *E*, respectively. The *inset* shows the effect of the time of ABTS addition on KatG catalatic O_2 production. ABTS was either present at time the reaction was initiated with H_2O_2 (*green*) or added 90 s (*red*), 180 s (*blue*), or 270 s (*black*) after initiation with H_2O_2. A reaction was also performed in which no ABTS was added (*gray*). The approximate time of ABTS addition is indicated by the *colored arrow* corresponding to each trace. All traces are representative of five repeated measurements.

Results

Inactivation of KatG during catalatic O_2 production

We monitored O_2 production by KatG upon reaction with 0.5 mM H_2O_2 at pH 5 (Fig. 2), the optimum for PxED-stimulated KatG catalase activity. Notably, the amount of O_2 produced (~0.1 mM, ~40% yield) was substantially below that anticipated from the 2 H_2O_2 to 1 O_2 stoichiometry of the catalase reaction. Addition of another 0.5 mM H_2O_2 at the conclusion of O_2 production did not result in any new O_2 generation, but a second addition of KatG produced a new burst of O_2 evolution. In contrast, inclusion of 0.1 mM ABTS (a PxED) in the reaction caused 10-fold higher rates of O_2 production as well as the H_2O_2 to O_2 stoichiometry expected from catalase activity. Furthermore, an additional injection of enzyme generated no new O_2, but addition of another 0.5 mM H_2O_2 resulted in new O_2 production. Thus, in the absence of ABTS, KatG was inactivated during turnover, leaving a substantial portion of H_2O_2 unreacted, but in the presence of ABTS, KatG remained active such that the H_2O_2 added to the reaction was completely depleted.

Catalase activity could be recovered by adding ABTS after H_2O_2; however, the longer KatG reacted with H_2O_2 in the absence of ABTS, the less activity could be recovered upon addition of ABTS (Fig. 2, *inset*). These data suggest that PxEDs intervene relatively early in the process of inactivation and prevent the accumulation of irreversibly inactivated KatG.

Conclusion of H_2O_2 consumption versus return of resting KatG

Optical stopped-flow reactions of 3 μM KatG with 667 molar eq of H_2O_2 at pH 5.0 showed that H_2O_2 consumption (240 nm)

Table 1
Catalase and peroxidase kinetic parameters of *Mt*KatG and W321F variant

Activity	KatG	Parameter			
		k_{cat}	k_{cat}/K_m	K_m	k_{app}
		s^{-1}	$M^{-1}\,s^{-1}$	mM	$M^{-1}\,s^{-1}$
Catalase (pH 7.0)[a]	*Mt*KatG	7600 ± 860	(1.0 ± 0.3) × 10^6	7.6 ± 2.4	
	W321F	7900 ± 110	(2.5 ± 0.1) × 10^6	3.2 ± 0.1	
Peroxidase[b] (H_2O_2)[c]	*Mt*KatG	17.6 ± 0.1	(5.2 ± 0.2) × 10^4	0.34 ± 0.01	
	W321F	9.9 ± 0.3[d]	(3.7 ± 0.9) × 10^4	0.27 ± 0.07	
Peroxidase (ABTS)[e]	*Mt*KatG	25.0 ± 0.1	(1.8 ± 0.1) × 10^5	0.14 ± 0.01	
	W321F	13.7 ± 0.1	(1.2 ± 0.2) × 10^5	0.11 ± 0.02	
Catalase (pH 5.0)[f] (no PxeD)	*Mt*KatG	170 ± 10	(2.8 ± 0.4) × 10^5	0.6 ± 0.1	(9.2 ± 0.3) × 10^3
	W321F	1680 ± 70	(1.5 ± 0.1) × 10^5	11 ± 2	
Catalase (pH 5.0)[f] (+0.1 mM ABTS)	*Mt*KatG	1400 ± 200	(3.0 ± 0.4) × 10^6	0.5 ± 0.1	
	W321F	4800 ± 500	(6 ± 1) × 10^5	8 ± 2	

[a] Activity was determined by H_2O_2 consumption observed at 240 nm at 23 °C in 100 mM phosphate buffer, pH 7.0.
[b] All peroxidase activity assays were performed at 23 °C in 50 mM acetate buffer, pH 5.0.
[c] Peroxidase parameters with respect to H_2O_2 were determined using 0.1 mM ABTS.
[d] Substrate-dependent inhibition observed ($K_{I(app)}$ = 3.3 ± 0.3 mM H_2O_2). Maximum observed $\nu_o/[E]_T$ ~6 s^{-1}.
[e] Peroxidase parameters with respect to ABTS were determined using 1.0 mM H_2O_2.
[f] Activity was determined by O_2 production at 23 °C in 50 mM acetate buffer, pH 5.0.

ceased at about 6 s, but more than 50 s were required for the ferric (*i.e.* resting) enzyme (408 nm) to completely reemerge. This slow return of the ferric state (k_{obs} ~0.055 s^{-1}) was not kinetically competent to account for the more than 500 molar eq of H_2O_2 consumed within the first 6 s of the reaction. These data indicate that catalase-inactive intermediates accumulate during turnover and that they are slow to return to the resting state.

wtKatG versus W321F: H_2O_2 consumption and corresponding heme states

Under typical catalase assay conditions (*i.e.* pH 7.0), our W321F KatG showed kinetic parameters nearly identical to the wild-type enzyme (Table 1). However, at pH 5.0, W321F KatG showed greater catalase activity, particularly at higher H_2O_2 concentrations. Reaction of W321F KatG with 2 mM H_2O_2 resulted in the same initial rate of H_2O_2 consumption as that observed for *wt*KatG (Fig. 3, *inset*). However, the rate of peroxide consumption decreased more rapidly for *wt*KatG than the W321F variant such that it took *wt*KatG roughly four times longer than W321F to consume a comparable quantity of H_2O_2. Furthermore, the return to the ferric state after H_2O_2 was consumed was nearly 10-fold faster for W321F (k_{obs} ~0.47 s^{-1}) than for *wt*KatG (k_{obs} ~0.055 s^{-1}) (Fig. 3).

Wild-type and W321F KatG showed nearly identical spectra 2.5 ms after mixing with 2.0 mM H_2O_2, including a Soret λ_{max} at 416 nm and Q band maxima at 542 and 578 nm (Fig. 4, *blue traces*). A notable feature of the spectrum relative to the enzyme's resting, ferric state is the lack of absorbance above 600 nm. The charge-transfer band, a hallmark of the ferric state, is absent and is *not* replaced by another absorption feature in spectra captured during KatG's most rapid catalatic H_2O_2 decomposition.

For *wt*KatG at the time corresponding to H_2O_2 depletion (6 s), the most obvious spectral change was a broad and substantial increase in absorption at wavelengths above 520 nm (Fig. 4*A*) with bands evident at 546 and 583 nm and a slight deflection at ~650 nm. There was also a small decrease in Soret band intensity at 416 nm. This same spectral progression has been

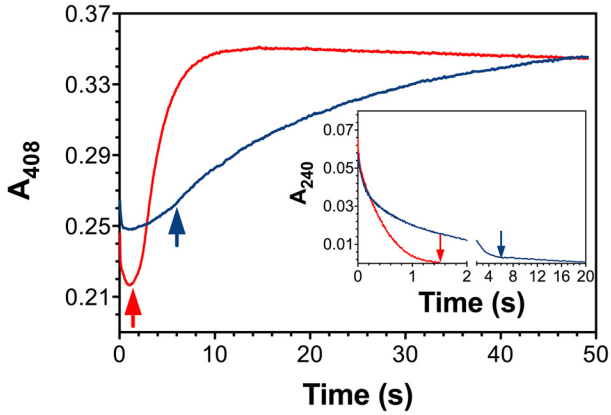

Figure 3. H_2O_2 consumption (*inset*) and return of the ferric state for *wt*KatG (*blue lines*) and W321F KatG (*red lines*). Reactions were carried out by stopped-flow, and after mixing they contained 3 μM enzyme and 2 mM H_2O_2. All reactions were carried out in 100 mM acetate, pH 5.0, at 4 °C. The *arrows* indicate the times in each trace corresponding to cessation of H_2O_2 consumption. Each *trace* represents an average of three shots. Data are representative of at least three repeated experiments.

observed across a range of KatGs upon reaction with H_2O_2 (38, 42). Therefore, a species whose features most closely resemble a Fe^{III}–O_2^- state dominates during the most rapid catalatic H_2O_2 consumption, and this gives way to a ferryl-like species that dominates at the time of H_2O_2 depletion. Indeed, a species with identical spectral features to the latter has been generated directly in several KatGs by reaction with peracetic acid (PAA) (42, 60, 61). This has been assigned through a combination of EPR and X-ray crystallographic studies as a ferryl-oxo (most likely protonated) species with a protein-centered radical where the proximal Trp has been identified as a prominent site of oxidation (*i.e.* Fe^{IV}–OH[Trp-321]‡ by *Mt*KatG numbering) (49, 56, 57).

Spectra observed for W321F KatG at its time of H_2O_2 depletion (Fig. 4*B*) were distinct from the wild-type enzyme. There was a substantial decrease in Soret intensity along with a blue-shift to about 410 nm. Similar to *wt*KatG, there was a broad nondescript increase in absorption intensity above 520 nm, but there were no distinct absorption bands at 546 and 583 nm, and the shoulder near 650 nm was more pronounced. These

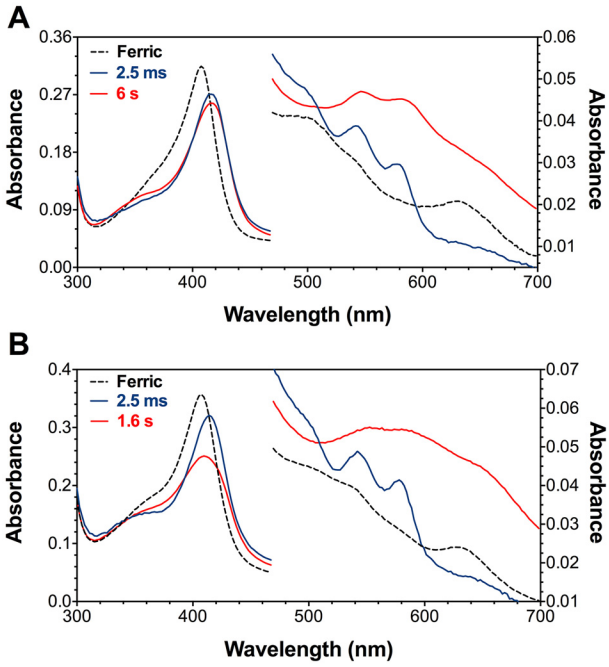

Figure 4. Spectra from reaction of wild-type and W321F KatG with H_2O_2. Wild-type (*A*) and W321F KatG (*B*) were reacted with 2 mM H_2O_2 by stopped flow, and spectra were recorded throughout the reaction by diode array. Spectra obtained 2.5 ms after reaction with H_2O_2 (*blue*) and at the time corresponding to H_2O_2 depletion (*red*) (6 s for wild-type and 1.6 s for W321F) are shown. Spectra recorded for the ferric enzyme following mixing with buffer alone are shown by *dashed lines*. All reactions were carried out as described for Fig. 3. Spectra are representative of at least three repeated experiments.

features have been observed in *M. tuberculosis* W321F KatG (and the equivalent variant from other species) following reaction with organic hydroperoxides (*e.g.* PAA) (60, 62). These features are consistent with a Fe^{IV}=O[porphyrin]$^{+}$ (*i.e.* compound I) species (25).

wtKatG protein-based radicals upon reaction with H_2O_2 alone

The EPR spectrum of *wt*KatG freeze-quenched after a 10-ms reaction time with H_2O_2 showed a complete loss of signals corresponding to the ferric heme (Fig. 5*A*) concomitant with formation of an intense doublet radical signal (Fig. 5*B*). Taking into account the partial power saturation of the radical signal at 4.5 K and 1 milliwatt of microwave power (Fig. 6*A*), this radical is in agreement with the so-called narrow doublet assigned by others as the cation radical of the MYW adduct (38–40). This same radical has been associated with the catalase activity of KatG (38, 40). Thus, our optical stopped-flow and rapid-freeze quench EPR are in accord with previous reports: the dominant steady-state intermediate of KatG catalase activity bears a MYW^{+} radical and a spectrum reminiscent of a Fe^{III}-O_2^{-} heme state.

At the time of H_2O_2 depletion (6 s), the ferric state was still absent (Fig. 5*A*), but the doublet radical was replaced by a singlet signal (Fig. 5*B*). In contrast to the narrow doublet, this signal was very broad (>300 G) (Fig. 6*B*), suggesting that there was exchange coupling with the heme iron. A very similar exchange-coupled radical species has been observed with KatG from *M. tuberculosis* and *Burkholderia pseudomallei* upon their reactions with PAA. In both cases, this radical has been assigned to the proximal Trp (Trp-321 and Trp-330, respectively) (56, 57).

When the reaction was quenched 1 min after mixing with H_2O_2, a signal corresponding to the ferric state (g ~6) was clearly present (although at diminished intensity compared with the resting state) (Fig. 5*A*) along with a singlet protein-based radical (Fig. 5*B*). Some broadening, although considerably less prominent than the species observed at 6 s, was evident (Fig. 6*B*). These data in addition to the power and temperature of the signal at 6 s (Fig. 6*C*) are consistent with multiple species being observed in both the 6-s and 1-min samples. In the 6-s sample, a large fraction of the observed signal arose from the exchange-coupled Trp-321 radical, and in the sample quenched at 1 min, the Trp-321 radical had migrated to more remote oxidizable amino acid residue(s).

The power saturation profiles for the narrow doublet, 6-s sample, and 1-min sample are shown in Fig. 6*D*. As expected, the MYW^{+} is very easily saturated under these conditions with a smaller $P_{½}$ of 6.4 μW. For the 6-s sample, the broad feature, measured at 3300 G, exhibits an extremely large $P_{½}$ of 16 milliwatts, consistent with its assignment to an exchange-coupled radical. If the power saturation of the 6-s sample is measured from peak-to-trough, the $P_{½}$ is ~12 μW, and the data show relatively poor fitting, suggesting that there are two overlapping signals here and that the 12-μW value should be regarded as an upper limit for $P_{½}$ for the second signal. The $P_{½}$ value of the sample quenched at 1 min is 7.5 μW, intermediate between the MYW^{+} and the organic radical seen in the 6-s sample and is indicative of a mixture of amino acid-based radicals.

In samples quenched 5 min after reaction with H_2O_2, a greater contribution from the ferric state (Fig. 5*A*) was observed along with a protein-based radical similar to that detected at 1 min albeit at lower intensity (Figs. 5*B* and 6*B*). Thus, freeze-quench EPR data are in good agreement with our stopped-flow results where the re-emergence of the ferric state is only observed after the depletion of H_2O_2 (at 6 s post-mixing), and the rate of return is too slow to account for the preceding catalatic consumption of >500 eq of H_2O_2. These data suggest that the primary catalase-inactive intermediate to accumulate contains a protein-based radical distinct from the MYW^{+} narrow doublet. The exchange coupling observed from this species is consistent with the proximal tryptophan (Trp-321) as the site of protein radical accumulation with subsequent radical migration away from the active site.

W321F KatG protein-based radicals formed upon reaction with H_2O_2 alone

Reaction of W321F KatG with the same concentration of H_2O_2 produced a nearly identical doublet radical spectrum at 10 ms (Fig. 5*C*). Similar to *wt*KatG, the narrow doublet was replaced by a protein-based singlet radical species at the time anticipated for the completion of H_2O_2 consumption (1.6 s for W321F *versus* 6 s for *wt*KatG). However, in contrast to the wild-type enzyme, the radical generated by W321F lacked any broadening that would indicate exchange coupling with the heme iron (Fig. 7*A*). Although a radical species was detected nearly a full minute later, its intensity in the variant was far less than that observed for the wild-type enzyme at the same time

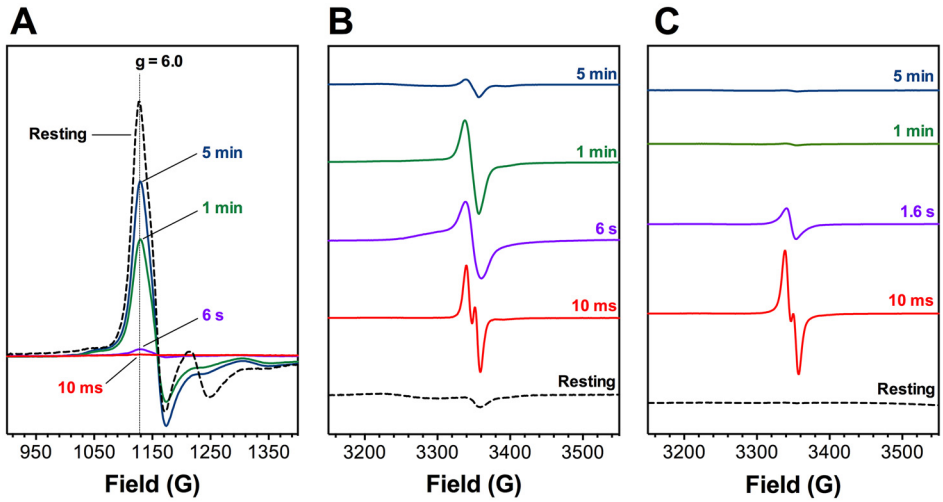

Figure 5. EPR spectra of freeze-quenched samples from reaction of WT and W321F KatG with H_2O_2. High-spin ferric species typical of the *wt*KatG resting state ($g\sim6$) are shown in *A*, the $g_{||}$ component of the resting state as well as protein-based radicals ($g\sim2$) of *wt*KatG and W321F KatG are shown in *B* and *C*, respectively. The molar proportions of enzyme to H_2O_2 used for stopped-flow experiments (1:667) were maintained for these experiments. Consequently, ferric enzyme (150 μM after mixing) was reacted with H_2O_2 (100 mM after mixing) for the time indicated prior to freeze-quenching. Reactions were carried out at 25 °C in 100 mM acetate, pH 5.0. All spectra were recorded at 4.5 K. Spectrometer settings were as described under "Experimental procedures." Freeze-quenched samples were generated at least twice with protein from different purifications. Spectra for a given time point were indistinguishable across both experiments.

point (Figs. 5*C* and 7*B*). Finally, where a weak radical signal was observed for the wild type even 5 min after H_2O_2 depletion, no radical was observed for W321F KatG at the same reaction time (Fig. 5*C*).

Effect of PxEDs on wtKatG and W321F

Inclusion of the PxED, ABTS, stimulated the consumption of H_2O_2 as well as the subsequent return of the ferric state of WT and W321F KatG; however, the effect was far more pronounced for WT (Fig. 8). Consistent with these data, we observed that ABTS increased the *wt*KatG catalase k_{cat} by 8-fold compared with only 3-fold for the W321F variant, with the same trend observed for k_{cat}/K_m (Table 1). We have noted previously that several PxEDs (*e.g.* 3,3′5,5′-tetramethylbenzidine) are able to stimulate *wt*KatG catalase activity to a level that equals or exceeds ABTS (55). These PxEDs all produced a significantly lower stimulation of W321F KatG catalase activity (data not shown).

To examine the effects of PxEDs on the intermediates formed for wild-type and W321F KatG, similar freeze-quench EPR experiments were performed as those presented above. With PxED (ABTS/ascorbate) included in the reaction mixture, WT and W321F KatG both showed the same narrow doublet 10 ms after mixing with H_2O_2 as was observed without PxED (Fig. 9, *A* and *B*). Spectra recorded for samples quenched at the time anticipated for H_2O_2 depletion or any time thereafter showed minimal, if any, contribution from protein-based radicals for either wild-type or W321F KatG (Fig. 9, *C* and *D*).

Discussion

Off-pathway electron transfer through Trp-321

Our data suggest that inactivation of KatG during catalatic consumption of H_2O_2 occurs due to off-pathway intramolecular electron transfer. Several lines of evidence suggest the proximal Trp (Trp-321 in *Mt*KatG) is a prominent site to initiate these radical transfer events. An exchange-coupled radical consistent with that previously assigned as Trp-321‡ (56, 57) accumulates and is the dominant radical as H_2O_2 consumption ceases. This signal is not observed when W321F KatG, an enzyme with robust catalase activity, is reacted with H_2O_2. The proximal Trp has been shown in several other contexts to be susceptible to oxidation. Reactions of KatGs with PAA routinely generate compound I species, which include a radical at this position (*e.g.* Fe^{IV}=O[Trp-321]‡ in *Mt*KatG) (56, 57). Calculations have shown that KatG compounds I (*i.e.* two-electron oxidized KatG) have substantial spin density associated with the proximal Trp, a result that is especially prominent when the arginine switch is oriented away from the MYW adduct (see *R418 out* in Fig. 1) (53). Interestingly, the out conformation for the arginine switch is known to increasingly dominate as the pH decreases below 6; this is where KatG has the greatest tendency toward inactivation and where we have observed that inclusion of a PxED shows the greatest stimulatory effect on KatG catalase activity. Finally, *Cc*P, one of KatG's closest superfamily relatives, forms the well-established compound ES (*i.e.* Fe^{IV}=O[Trp-191]‡) upon reaction with H_2O_2 (58, 59), where Trp-191 is *Cc*P's proximal Trp (see Fig. 1).

Scavenging of off-catalase KatG protein-based radicals by PxEDs

A variety of PxEDs do not inhibit but instead substantially stimulate KatG catalase activity (55). Accordingly, we show here that inclusion of a PxED does not diminish (if anything, it enhances) the formation of the MYW adduct radical associated with catalase turnover, not only in *wt*KatG, but also in the W321F variant. This confirms what has been surmised from KatG's very narrow active-site access channel (20–22). Specifically, PxEDs like ABTS cannot directly access the active site, but rather must act from some exterior site(s).

Strikingly, PxEDs essentially abrogate the accumulation of all other protein radical species. This includes the exchange-coupled Trp-321‡ radical; those that are observed well after H_2O_2

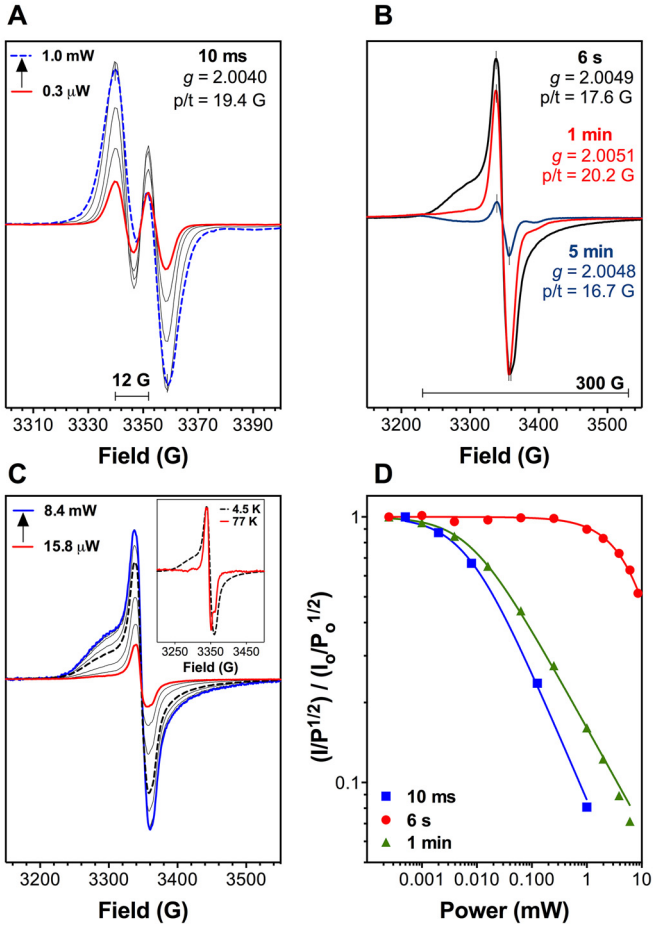

Figure 6. Evaluation of protein-based radicals detected during *wt*KatG reaction with H_2O_2. The doublet radical observed 10 ms after mixing with H_2O_2 (*A*) was recorded across a range of microwave power settings from 0.3 μW (*solid red line*) to 1.0 milliwatt (*dashed blue line*). The radicals observed 6 s (*black line*), 1 min (*red line*), and 5 min (*blue line*) after mixing with H_2O_2 all recorded using a microwave power of 1.0 milliwatt are compared (*B*), and the *g* value and peak-to-trough (*p/t*) width of each radical are indicated. The effect of microwave power (15.8 μW (*red line*) to 8.4 milliwatt (*blue line*)) on the spectrum recorded for the sample quenched 6 s after *wt*KatG reaction with H_2O_2 is shown (*C*). The spectrum recorded with 1.0 milliwatt microwave power (*dashed black line*) is highlighted in the *main figure* and scaled for comparison with the spectrum recorded at 77 K using the same power (*inset*). The normalized signal intensities for samples collected 10 ms, 6 s, and 1 min after *wt*KatG reaction with H_2O_2 as a function of microwave power are shown in *D*. Unless otherwise indicated, all spectra were recorded at 4.5 K with all other spectrometer settings as described in "Experimental procedures." Samples were prepared and evaluated as described for Fig. 5.

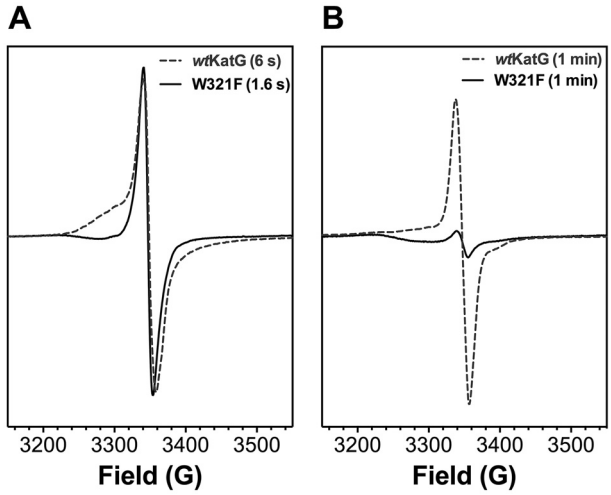

Figure 7. Comparison of EPR spectra for W321F and *wt*KatG at and after the cessation of H_2O_2 consumption. The radical observed for W321F (*solid line*) at the time of H_2O_2 depletion (1.6 s) is compared with that recorded for wild-type KatG (*dashed line*) at the analogous time (6 s) (*A*). The radical observed for W321F (*solid line*) and wild-type (*dashed line*) 1 min after mixing with H_2O_2 is also shown (*B*). Sample preparation, reaction conditions, and spectrometer settings are the same as those described for Fig. 5.

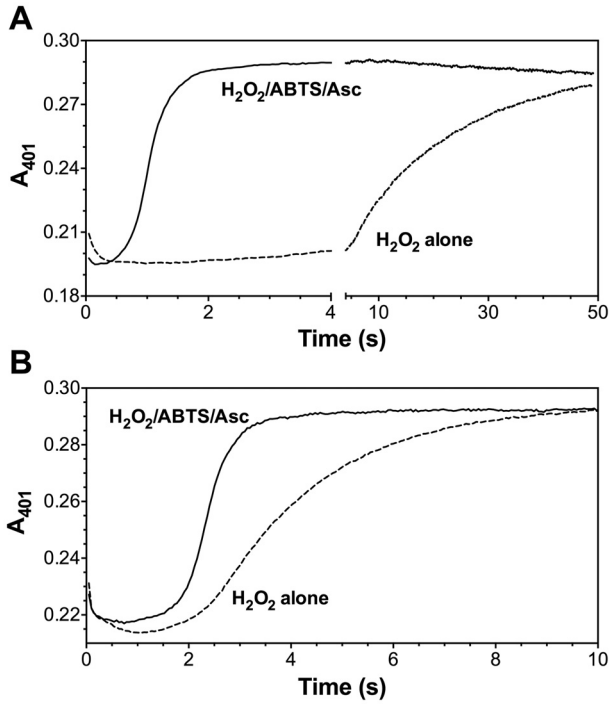

Figure 8. Effect of ABTS on the return of the KatG ferric state following H_2O_2 consumption. Wild-type (*A*) and W321F KatG (*B*) were reacted by stopped flow with 2.0 mM H_2O_2 in the absence and presence of 0.1 mM ABTS, 0.1 mM ascorbate. The return of the ferric state following H_2O_2 depletion was monitored at 401 nm. The final concentration of enzyme in each reaction was 3 μM. All reactions were carried out in 50 mM acetate buffer, pH 5.0, at 4 °C. Data are representative of at least three repeated experiments.

consumption has ceased, and the alternative radical species that are detected when W321F KatG reacts with H_2O_2. Combined with its inability to reduce the $MYW^{+\cdot}$ radical directly, this implies that PxED (*e.g.* ABTS) oxidation occurs by a through-protein electron hole-hopping mechanism. Consequently, PxED oxidation (and by extension peroxidase activity) requires a preceding off-catalase radical transfer event, the first step of which appears to be oxidation of the proximal Trp. This mechanism produces an interesting reciprocity between KatG's catalase and peroxidase activities. Off-catalase electron transfers result in PxED oxidation (*i.e.* peroxidase activity), which simultaneously reduces protein radicals and prevents further protein oxidation. This ultimately preserves catalase activity to enable the full depletion of H_2O_2. Indeed, our data show that in the presence of ABTS, there is no loss of activity even following 50,000 turnovers per active site (Fig. 2). Interestingly, PAA-dependent isoniazid (INH) oxidation by *Mt*KatG also appears to be mediated by an electron hole-hopping mechanism and to occur at or near the protein surface (56). This raises the intriguing possibility that in the presence of the physiological substrate

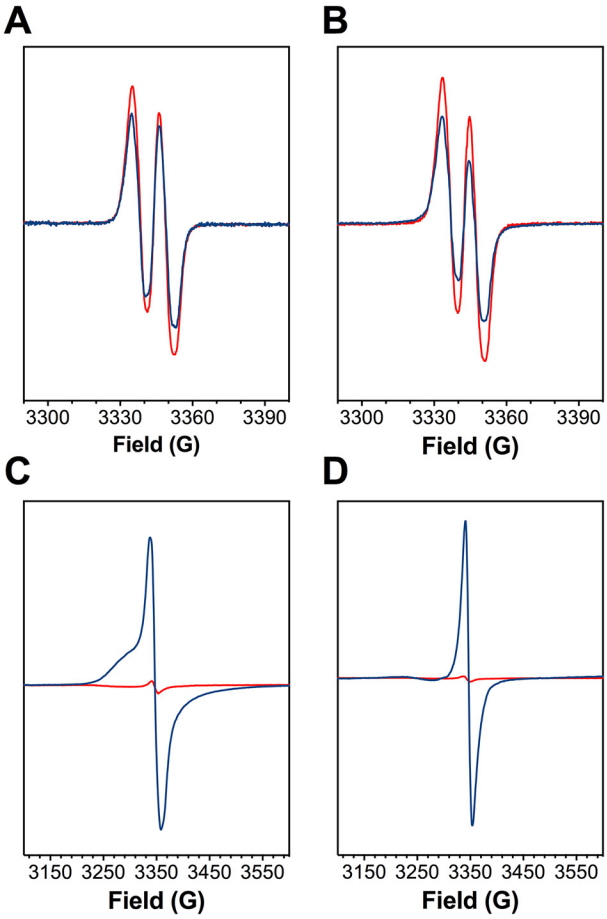

Figure 9. Comparison of EPR spectra for protein-based radicals 10 ms after mixing with H_2O_2 (*A* and *B*) and at H_2O_2 depletion (*C* and *D*). Spectra were recorded for *wt*KatG (*A* and *C*) and the W321F variant (*B* and *D*) in the absence (*blue lines*) and presence of ABTS/ascorbate (*red lines*). Reaction conditions, sample preparation, and evaluation were as described for Fig. 5. When included, the concentrations of ABTS and ascorbate were 1.0 and 2.0 mM, respectively. Spectra shown in *A* and *B* (10 ms after mixing with H_2O_2) were recorded at 77 K, minimizing power saturation of the radical observed at 4.5 K (see Figs. 5, *B* and *C*, and 6*A*). Spectra shown in *C* and *D* (at the time of H_2O_2 depletion) were recorded at 4.5 K. All spectrometer settings were as described under "Experimental procedures."

H_2O_2, INH activation may be facilitated by the synergistic cooperation of KatG's catalase and peroxidase activities

KatG protein oxidation in the absence of a PxED

Of course, through-protein electron hole-hopping occurs during H_2O_2 decomposition by KatG even in the absence of a PxED. Such is evident in our EPR spectra as the exchange-coupled W321‡ observed at the time of H_2O_2 depletion is replaced at later reaction times by radicals that lack a close interaction with the heme iron. Similarly, at temperatures where the exchange-coupled W321‡ signal is not detected (*e.g.* 77 K), EPR spectra reveal that more remote protein-based radicals are also present at the time of H_2O_2 depletion (Fig. 6*C*, *inset*). An essentially identical phenomenon has been observed when KatG is reacted with PAA (56). It is important to bear in mind that PAA is a hydroperoxide that cannot support the full catalase cycle, and as such it makes off-catalase electron transfer unavoidable.

More than this, the structure of KatG is one that almost seems to *invite* through-protein radical migration. The active-site-bearing N-terminal domain has an extraordinarily high content of oxidizable amino acid side chains (18 Trp, 4.2%; 16 Tyr, 3.7%; 14 Met, 3.2%; 2 Cys, 0.5%; 50 total, 11.6%). Hole-hopping electron transfer has recently been proposed and explored as a broadly used strategy for preserving the activity of redox enzymes (63–65); it is one that KatG appears particularly well-equipped to utilize. Indeed, reactions of KatGs with peroxides are known to generate a variety of protein-based radicals and a range of advanced protein-oxidation products. As summarized in Fig. 10*A*, these include radicals identified in at least one KatG at the equivalent of Trp-91, Trp-135, Trp-321, and Trp-149 (56, 57, 66) as well as oxygenation of Trp-438, Trp-149, Trp-135, Met-377, Met-255/257, and Met-176 (61). Similarly, oxidative cross-linking/oligomerization has been observed, ostensibly arising from exterior Tyr- and/or Trp-based radicals (39, 67). It is reasonable to surmise that sacrificial KatG protein oxidation may substantially prolong catalatic H_2O_2 decomposition, but our data show that in the absence of a PxED, KatG eventually undergoes irreversible inactivation. Under the conditions of Fig. 2 (*i.e.* 0.5 mM H_2O_2, pH 5.0), 5 nM KatG generated 100 μM O_2 over the course of the reaction, indicating that irreversible inactivation occurred after roughly 20,000 turnovers.

Functional significance of redox chain overlap: KatG and CcP

Using the algorithms of Gray and Winkler (63), we note that the large majority of KatG residues known to undergo oxidative modification fit into one of four redox chains (Fig. 10*A*). In the context of this study, the chain that includes Trp-321 is particularly interesting. As one of KatG's closest relatives, C*c*P is also rich in oxidizable amino acids (Trp + Tyr + Met + Cys = 27 or 9.2%). Nevertheless, there is a surprising lack of conservation of oxidation sites with only 11 in common between the two enzymes, including four instances where Trp replaces Tyr or vice versa (Fig. 10, *B* and *D*). Interestingly, seven of the conserved oxidation sites are found proximal to the active-site heme. Among these, an electron hole-hopping path can be discerned that connects to the enzyme's surface and includes Trp-321 (heme–Trp-321–Met-377–Tyr-353 and/or Trp-341) (Fig. 10*A*). The proximal Trp has been observed in both proteins to be oxidized to a radical intermediate (56–58). Met-377 (Met-231 in C*c*P) lies 3.9 Å from the proximal Trp, and in both KatG (61) and C*c*P (65), this Met is oxygenated upon reaction with peroxides. Both Tyr-353 (Trp-223 in C*c*P) and Trp-341 (Trp-211 in C*c*P) form part of a shallow solvent-accessible cleft ~17 Å below the heme plane. In C*c*P, both Trp-223 and Trp-211 are oxygenated following the enzyme's reaction with H_2O_2 (65), and in *Mt*KatG, NO has trapped a radical centered at Tyr-353 (68).

The conservation of this electron transfer conduit points to use of a shared electron transfer structure to support divergent redox protein function. Of course, C*c*P is a monofunctional peroxidase, but it is unique in the peroxidase-catalase superfamily in that it uses a large protein-based substrate (ferrocytochrome *c*) as a PxED. This precludes direct access of the substrate to the C*c*P heme and necessitates through-protein radical transfer, which includes the enzyme's proximal tryptophan (Trp-191). In the case of KatG, PxEDs are precluded from access to the heme because the channel to the active site is

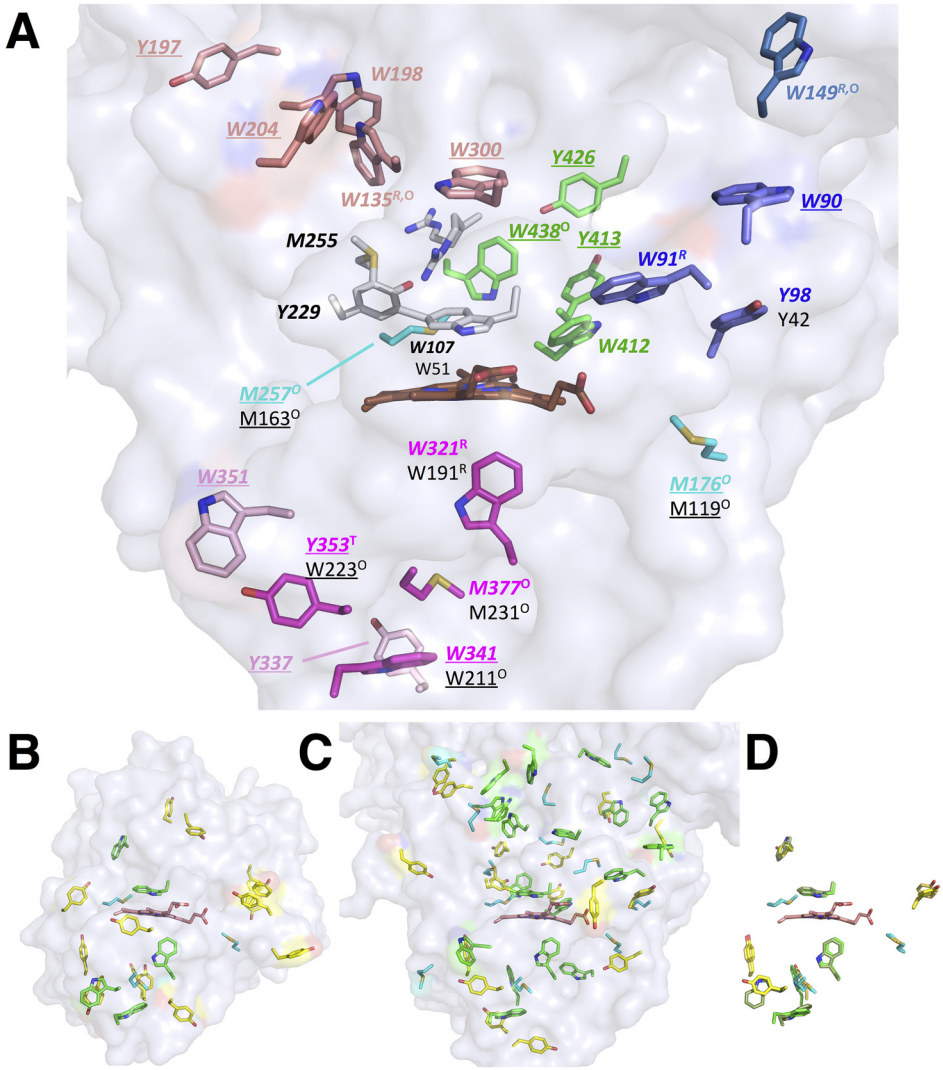

Figure 10. Oxidizable amino acids in KatG and CcP. Potential routes for off-catalase electron transfer in KatG compared with sites of peroxide-dependent protein oxidation in KatG and CcP are shown in *A*. Four principal pathways are proposed. With respect to KatG, the *magenta path* connects to the heme via the proximal Trp (*W321*). The *green path* connects to the heme via Trp-412. The *blue path* connects to the heme via Trp-91. The *copper-colored path*, which includes Trp-135, is purported to connect to the heme via the MYW adduct Trp (*W107*). Solvent-exposed side chains are *underlined*. Residues identified in *bold italics* belong to KatG, and oxidizable sites conserved in CcP are indicated in *regular typeface*. Residues with *superscript designations* are sites where oxidative modifications have been observed as follows: a radical intermediate has been directly observed (*R*) (56–59, 66) or trapped (*T*) (68) or side chain oxygenation has been detected (*O*) (61, 65). Placement of tryptophan (*green*), tyrosine (*yellow*), and methionine (*cyan*) residues in CcP (2CYP) (24) and the KatG N-terminal domain (2CCA) (78) are shown in *B* and *C*, respectively. An overlay of conserved oxidizable amino acids is shown in *D*, where *drab shades* represent residues from CcP, and *bright shades* represent residues from KatG.

particularly narrow. As mentioned above, this permits the mutually synergistic or reciprocal operation of the catalase and peroxidase activities of KatG. With either enzyme, in the absence of an appropriate PxED, the protein itself becomes an electron source to forestall, for a limited time, irreversible inactivation.

Integrating KatG catalysis: catalase, peroxidase, inactivation, and PxED-based recovery

A model summarizing our observations is presented in Fig. 11. Following its formation (paths a), the dominant pathway for reaction of compound I (*i.e.* Fe^{IV}=O[porphyrin]$^{+}$) is formation of compound I* (*i.e.* Fe^{IV}=O[MYW]$^{+}$) and the subsequent catalatic oxidation of H_2O_2 (paths b). Occasionally (about once every 140 turnovers), the porphyrin radical is instead reduced by the proximal Trp (Trp-321) to form Fe^{IV}=O[Trp-321]$^{+}$ (reactions c). Indeed, with relatively few equivalents of H_2O_2 (~650), Trp-321^{+} accumulates and is the dominant radical species at the time of H_2O_2 depletion (see Figs. 5*B* and 6*B*). This is mirrored by a previous report showing a decrease in MYW^{+} signal with time during reactions with H_2O_2 (38). KatG's catalase activity exceeds its peroxidase activity by about 2 orders of magnitude. We have noted that KatG "peroxidase activity" may be more accurately described as a PxED-dependent stimulation of catalase activity, a mechanism that requires relatively infrequent PxED oxidation (*e.g.* 0.007 ABTS^{+} generated for every H_2O_2 consumed) (55). Based on our present results, we suggest that each PxED oxidation event (*e.g.* ABTS^{+}) reports correction of off-catalase radical transfer. As such, we estimate that the frequency of catalatic H_2O_2 oxidation (paths b) *versus* off-catalase radical transfer (paths c) is about 140 to 1.

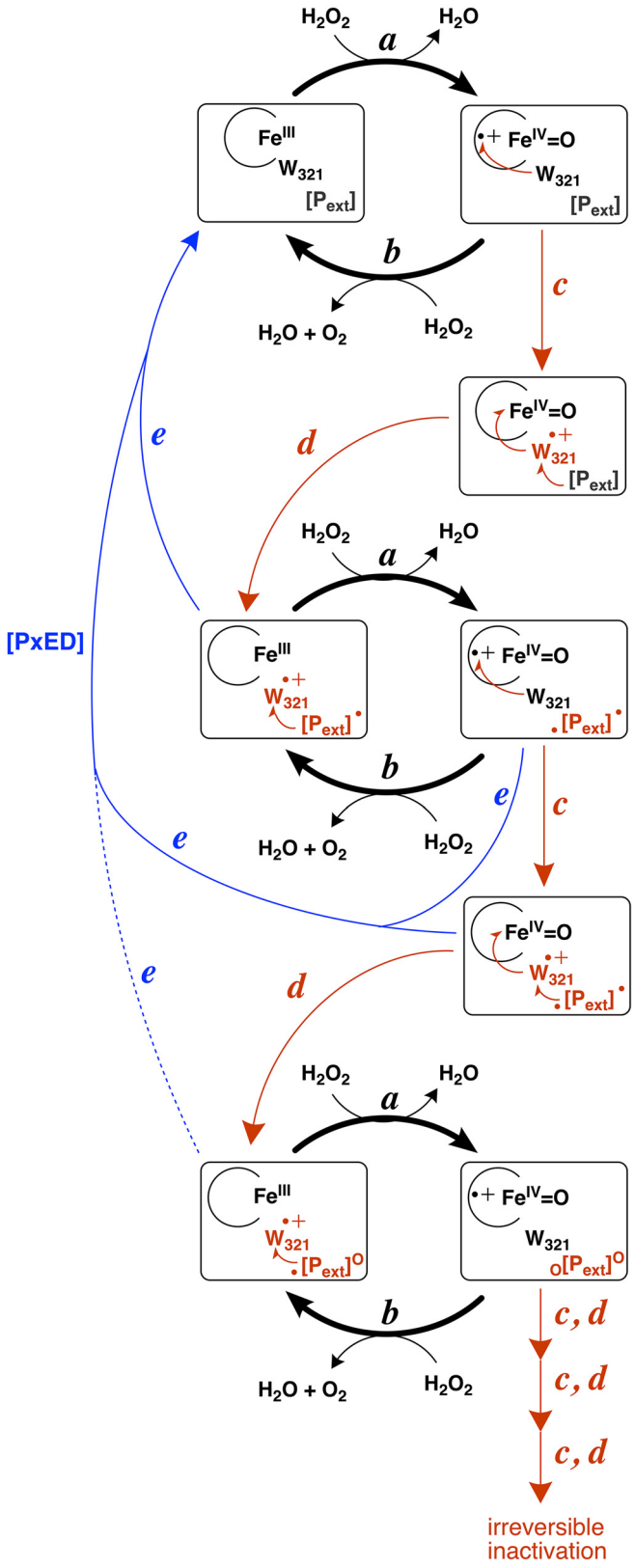

Figure 11. Proposed mechanism for inactivation of KatG catalase and its prevention by a PxED. The KatG catalase cycle is initiated by H_2O_2 oxidation of ferric heme to the compound I (*i.e.* Fe^{IV}=O[porphyrin]$^{+}$) state (*reactions a*). The catalatic return of compound I to the ferric state (abbreviated from Fig. 1) proceeds by *paths b*, the first step of which is the oxidation of the MYW adduct to its radical cation state (*MYW*$^{+}$) (not shown). Alternative off-catalase oxidation of the proximal Trp (W_{321}) is shown by *reactions c*. The relative *thickness* of the *arrows* for *b versus c* indicates that MYW oxidation and subsequent completion of the catalase cycle (*b*) occurs with a much greater frequency than Trp-oxidation (*c*) (~140:1). The return of ferric heme following off-catalase electron transfer occurs by hole-hopping (*i.e.* radical transfer indicated by *red half-arrows*) to KatG-oxidizable residues more distant from the active site ([P_{ext}]), producing the corresponding protein-based radicals ([P_{ext}]$^{\cdot}$) (*paths d*). Horizontal transitions correspond to catalase activity. Each *vertical transition* is a step in the progressive oxidation of the KatG protein. In the early stages protein-based radicals are the dominant oxidation intermediates, as vertical steps continue, more advanced oxidation products ([P_{ext}]^{O} and $_{O}$[P_{ext}]^{O}) accumulate, including oxygenated Trp and Met, cross-linked Tyr, oxidative protein aggregates, etc. Conceivably, catalase activity can still be maintained even though the KatG protein has sustained some level of exterior oxidation, but eventually, enzyme inactivation results. Inclusion of a PxED intercepts and reduces protein-based radicals on the KatG surface (*e*), preventing/reversing vertical progression toward inactivation.

Radical transfer away from the active site toward the KatG surface (paths d) regenerates the ferric heme, which can then engage in additional catalase turnover (paths a and b). Consistent with this notion, remote protein-based radicals are observed at later times as the ferric state slowly returns (Fig. 5*B* and 6*B*). Additional turnover produces additional iterations of off-pathway electron transfer, resulting in advanced protein oxidation products. In our reaction scheme, this is represented as a vertical descent via repeated iterations c and d.

Our data suggest that it is a ferryl heme from which the ferric state returns upon depletion of H_2O_2. The spectrum that progressively develops as catalatic H_2O_2 consumption proceeds (Fig. 4*A*) is indistinguishable from the Fe^{IV}-OH[protein]$^{\cdot}$ state that is directly generated when KatGs are reacted with organic hydroperoxides (42, 49, 56, 57, 60). The slow recovery of the resting state from these ferryl states is anticipated, particularly as protein-based electron sources become depleted through oxygenation and other oxidative modifications (*i.e.* vertical descent in Fig. 11 through repeated exploitation of paths c and d). With the relatively low H_2O_2 concentration examined by stopped-flow (667 molar eq), the ferric state returns with a k_{obs} of about 5.5×10^{-2} s^{-1} (see Fig. 3). Notably, when a PxED is present during H_2O_2 consumption, little if any ferryl state accumulates, instead, the Fe^{III}-$O_2^{\cdot-}$-like spectrum of the catalase active state reverts rapidly and directly to ferric KatG (55).

A PxED, when present, does not directly access the active site. Rather a radical transfer pathway(s) delivers oxidizing equivalents via Trp-321 to an exterior site(s) where electron transfer from the PxED to protein radicals (Trp$^{\cdot}$, Tyr$^{\cdot}$, etc.) can occur (Fig. 11, *paths c* to *d* to *e*). Consequently, a PxED is effective at remediating the early stages of KatG protein oxidation, preventing progression to advanced/irreversibly oxidized states. Indeed, the capacity of a PxED to recover KatG catalase activity upon its addition diminishes exponentially the longer KatG reacts with H_2O_2 alone (see Fig. 2, *inset*).

All our data point toward the proximal tryptophan (Trp-321) as the primary starting point for off-catalase electron transfer. Although substantially less than wild type, PxEDs do show a modest stimulatory effect on W321F catalase activity, and remote protein-based radicals are detected in this protein at the cessation of H_2O_2 consumption. This indicates that other pathways of off-mechanism radical transfer may be explored albeit at a slower rate/lesser extent in the absence of Trp-321.

In conclusion, the KatG proximal Trp-321 is a starting point for off-catalase radical transfer, the continuation of which even-

tually produces advanced protein oxidation and irreversible inactivation. However, with a PxED present, radicals transferred by electron hole-hopping via the proximal Trp to the enzyme surface are reduced. This indefinitely preserves KatG catalase activity and simultaneously produces KatG peroxidase activity, greatly increasing the capacity of the enzyme to degrade H_2O_2. Given the wide use of KatGs by plant and animal pathogens and the pivotal role that PxEDs could play in KatG-dependent detoxification of host-derived H_2O_2, this phenomenon may hold important implications for understanding host–pathogen interactions.

Experimental procedures

Materials

Ampicillin, H_2O_2 (30%), hemin, imidazole, calcium chloride hydrate, sodium dithionite, ABTS, 3,3′-dimethoxybenzidine (*o*-dianisidine), *N,N,N′,N′*-tetramethyl-*p*-phenylenediamine dihydrochloride, 3,3′,5,5′-tetramethylbenzidine dihydrochloride hydrate, chlorpromazine, pyrogallol, and L-ascorbic acid were from Sigma. Mono- and dibasic sodium phosphate, sodium acetate trihydrate, sodium chloride, potassium chloride, magnesium sulfate, magnesium chloride, and tetracycline hydrochloride were purchased from Fisher. T4 DNA ligase, *Pfu* polymerase, and *Escherichia coli* (XL-1 Blue) were obtained from Agilent (La Jolla, CA). All oligonucleotide primers were purchased from Invitrogen. All restriction enzymes and Phusion high-fidelity PCR master mix with GC Buffer were obtained from New England Biolabs (Beverly, MA). Bugbuster, Benzonase nuclease, and nickel-nitrilotriacetic acid resin were obtained from Novagen (Madison, WI). Isopropyl β-D-thiogalactopyranoside was obtained from Gold Biotechnology (St. Louis, MO). Macro-Prep High Q resin and Buffer Exchange columns (10DG) were purchased from Bio-Rad. Centrifugal filter units (50-kDa cutoff) were acquired from Millipore (Billerica, MA). All buffers and media were prepared using water purified through a Barnstead EASYpure II UV ultrapure water system (18.2 megohms/cm resistivity).

Mutagenesis

Site-directed mutagenesis was carried out by applying the "Round-the-Horn" approach (69) to the construct we use for the expression of wild-type *Mt*KatG. This construct, pMRLB11, is a pET23b-derived plasmid bearing the *M. tuberculosis katG* gene and was obtained from the TB Vaccine Testing and Research Materials Contract at Colorado State University. The sense strand primers designed for W321F substitution (5′-GAG*GTG*GTA**TTT**ACGAACACCCCGACGAAATGG-GAC-3′) included a site for codon replacement (bold) as well as mutations designed to introduce diagnostic restriction digest sites for screening (italics). This approach allowed us to generate reverse primers without substitutions for W321F 5′-GAT-GCCGCTGGTGATCGCGTCCTTACCG-3′. Both primers were modified by 5′-phosphorylation to allow for blunt-end ligation of PCR products. PCR for generation of the variant was carried out using Phusion High Fidelity polymerase (New England Biolabs, Beverly, MA) in GC Buffer-containing master mix and 3% DMSO. The PCR products were treated with DpnI to eliminate the starting template and ligated using T4 DNA ligase. The ligation products were used to transform *E. coli* (XL-1 Blue) by a standard heat-shock procedure. Transformants were selected using ampicillin-containing media, and candidate plasmids were screened by BsaAI restriction digest. Successful candidates were sent for full DNA sequence analysis (Davis Sequencing, Davis CA) to verify that the intended mutations were present and that no unintended mutations were generated.

Protein expression and purification

E. coli C41(DE3) cells bearing the heme protein expression plasmid pHPEX3 (70) were transformed with the appropriate expression construct, and transformants were selected on the basis of tetracycline/ampicillin resistance. Expression of wild-type *Mt*KatG and all variants was carried out as described previously (55). As with wild-type *Mt*KatG, the W321F variant was expressed in a soluble form. Thus, purification was carried out as reported previously (55), with the exception that lysis was carried out by sonication. A Branson 250 sonifier (Danbury, CT) fit with a standard tip was set to constant output and 3.5 duty. Sonication was carried out in eight cycles (42 s on, 42 s off). Benzonase nuclease (250 units) was added to the lysate following sonication.

UV-visible spectra and activity assays

Following purification, UV-visible spectra for WT and W321F *Mt*KatG (3 μM each) were evaluated in 100 mM phosphate, pH 7.0, as described previously (55). Molar absorptivities were determined using the pyridine hemichrome assay (71). For WT and W321F KatG, optical purity ratios A_{408}/A_{281} (*i.e.* $R_Z = 0.62$), the absorption maxima for the Soret band (λ_{max} = 408 nm), and the two charge-transfer bands (CT2 λ_{max} = 500 nm; CT1 λ_{max} = 633 nm) were indistinguishable.

Peroxidase activity was evaluated as described previously (55) by monitoring ABTS (the PxED) oxidation to $ABTS^{\ddagger}$ ($\epsilon_{417} = 34.7\ mM^{-1}\ cm^{-1}$) (72). To evaluate the effect of H_2O_2 concentration on peroxidase activity, ABTS was held constant at 0.1 mM. To determine the effect of ABTS concentration, H_2O_2 concentration was held constant at 1.0 mM. All peroxidase assays were carried out at room temperature in 50 mM acetate, pH 5.0. The concentration of the enzyme used in all assays was 20 nM.

Unless otherwise specified, catalase activity was evaluated by monitoring O_2 production over time using a Clark-type O_2-sensitive electrode (Hansatech, Pentney, Norfolk, UK) as described previously (55). In specified experiments, catalase activity was evaluated spectrophotometrically by monitoring a decrease in H_2O_2 concentration over time at 240 nm ($\epsilon_{240} = 39.4\ M^{-1}\ cm^{-1}$) (73). Analyses of steady-state kinetic data were carried out as described previously (55). As before, *wt*KatG catalase activity showed a two-component response to H_2O_2 at pH 5, necessitating the use of Equation 1,

$$v_o/[E]_T = \frac{k_{cat}[H_2O_2]}{k_{cat}/k_{on} + [H_2O_2]} + k_{app}[H_2O_2] \qquad \text{(Eq. 1)}$$

which permits determination of the apparent second-order rate constant (k_{app}) for a "high K_m" response to H_2O_2. In addition,

data were fit to directly estimate k_{cat}/K_m (indicated as k_{on} in Equation 1) and k_{cat}. In all other instances, a second "high K_m" component was not observed, and data were fit to Equation 2.

$$v_o/[E]_T = \frac{k_{cat}[H_2O_2]}{k_{cat}/k_{on} + [H_2O_2]} \quad \text{(Eq. 2)}$$

Stopped-flow

Heme intermediates formed by WT and W321F *Mt*KatG under steady-state conditions were observed using a PC-upgraded SX18.MV rapid reaction analyzer from Applied Photophysics (Leatherhead, UK). As described previously (55), to more clearly observe absorption due to heme intermediates, we included ascorbate to scavenge the radical oxidation products of PxEDs (*e.g.* $ABTS^{\cdot+}$) (55, 74, 75). Single-mixing experiments were set up such that 6 μM wild-type or W321F KatG was placed in syringe A in 5 mM phosphate buffer, pH 7.0. Syringe B contained 0.2 mM ascorbate, 0.2 mM ABTS, and varying concentrations of H_2O_2 in 100 mM acetate buffer, pH 5.0.

Freeze-quench preparation of EPR samples

Wild-type and W321F KatG were each concentrated to ~300 μM using an Amicon Ultra-4 centrifuge filter (cutoff at 50 kDa). One syringe contained ~300 μM enzyme in 5 mM phosphate, pH 7.0, and the other syringe contained 667 molar eq of H_2O_2 in 100 mM acetate buffer, pH 5.0. Reactions testing the impact of PxED included ABTS (2.0 mM) and ascorbate (4.0 mM) along with H_2O_2.

EPR samples were prepared by mixing equal volumes of solution from each syringe. Each reaction was quenched by freezing after the appropriate time following mixing. Samples frozen less than 1 s after mixing were quenched by spraying the reaction mixture directly into liquid ethane (−150 °C) by a standard rapid quench procedure using a System 1000 Chemical/Freeze Quench Apparatus (Update Instruments, Inc.), and the reaction time was determined by the length of the aging loop and velocity of the motor driving the syringes. For reactions between 1 and 30 s, the samples were still quenched with liquid ethane; however, a modified flow-pause-flow freeze-quench procedure was used in which the quenching time was determined by the pause duration. For reaction times longer that 30 s, reactions were initiated by hand mixing. The samples were centrifuged to remove excess bubbles from O_2 production, transferred to quartz EPR tubes, and quenched manually in cold isopentane (−130 °C). All samples were stored in liquid N_2 until analyzed by EPR spectroscopy.

EPR measurements

All X-band (9 GHz) EPR spectra were collected using either a Bruker ER200D or an EMX spectrometer operating in perpendicular mode at 100 kHz modulation frequency in a 4119HS resonator. The spectrometer was equipped with an ESR910 liquid helium cryostat and an ITC503S temperature controller (Oxford Instruments), and spectra were recorded at 4.5 K and/or 77 K. For spectra recorded at 4.5 K instrument parameters, unless otherwise indicated, were as follows: microwave frequency, 9.393 GHz; modulation amplitude, 2 G; modulation frequency, 100 kHz; microwave power, 1 milliwatt; time constant, 163.84 ms; sweep time 335.54 s; number of scans, 1; conversion, 327.68 ms; resolution, 1024 point; harmonic 1st; receiver gain, 1.0×10^4; and phase, 0 degrees. For spectra recorded at 77 K, all parameters were the same except the modulation amplitude was 1 G, the receiver gain was 1.0×10^5, and the microwave power was 15.84 μW.

Power saturation for select species was examined by fitting normalized signal intensities using Equation 3,

$$(I/\sqrt{P})/(I/\sqrt{P})_o = 1/(1 + P/P_{1/2})b/2 \quad \text{(Eq. 3)}$$

where $P_{1/2}$ is the microwave power at half-saturation, and b describes the contribution from inhomogeneous broadening (76). For the signal we observed for *wt*KatG in reactions quenched 6 s after mixing with H_2O_2, signal intensities at 3300 G as well as peak-to-trough were evaluated. The former was to isolate the contribution of the exchange-coupled species.

Author contributions—O. J. N. and D. C. G. designed and interpreted the experiments. O. J. N. carried out site-directed mutagenesis (W321F), protein expression, and purification. O. J. N. performed steady-state and stopped-flow kinetic analyses. E. N. N. carried out refinement of the stopped-flow procedures used in this report. J. R. K. designed, performed, and evaluated the extent of O_2 production by wild-type KatG. O. J. N. and I. D. performed freeze-quench sample preparation, and the initial EPR evaluation was carried out in the lab of A. L., O. J. N., and I. D. collected EPR spectra, first at Georgia State University and subsequently at Auburn University. I. D. and A. L. assisted with interpretation of EPR spectra and power saturation properties of the radicals observed. The manuscript was written by O. J. N. and D. C. G. with consultation from I. D., J. R. K., A. L., and E. N. N. All authors reviewed the results and approved the final version of the manuscript.

Acknowledgments—We thank Dr. Jay Winkler for assistance with the Protein Electron Transfer Database. We thank our colleagues Drs. Holly Ellis and Steve Mansoorabadi for helpful discussions, and Dr. Evert Duin for assistance with the EMX EPR spectrometer.

References

1. Zamocky, M., and Obinger, C. (2010) in *Biocatalysis Based on Heme Peroxidases* (Ayala, M., and Torres, E., eds) pp. 7–35, Springer-Verlag, Berlin
2. Mishra, S., and Imlay, J. (2012) Why do bacteria use so many enzymes to scavenge hydrogen peroxide? *Arch. Biochem. Biophys.* **525,** 145–160
3. Imlay, J. A. (2008) Cellular defenses against superoxide and hydrogen peroxide. *Annu. Rev. Biochem.* **77,** 755–776
4. Tanabe, S., Ishii-Minami, N., Saitoh, K., Otake, Y., Kaku, H., Shibuya, N., Nishizawa, Y., and Minami, E. (2011) The role of catalase-peroxidase secreted by *Magnaporthe oryzae* during early infection of rice cells. *Mol. Plant Microbe Interact.* **24,** 163–171
5. Uhlich, G. A. (2009) KatP contributes to OxyR-regulated hydrogen peroxide resistance in *Escherichia coli* serotype O157: H7. *Microbiology* **155,** 3589–3598
6. Uhlich, G. A., Chen, C. Y., Cottrell, B. J., Irwin, P. L., and Phillips, J. G. (2012) Peroxide resistance in *Escherichia coli* serotype O157:H7 biofilms is regulated by both RpoS-dependent and -independent mechanisms. *Microbiology* **158,** 2225–2234
7. Passardi, F., Zamocky, M., Favet, J., Jakopitsch, C., Penel, C., Obinger, C., and Dunand, C. (2007) Phylogenetic distribution of catalase-peroxidases: are there patches of order in chaos? *Gene* **397,** 101–113
8. Zhang, Y., Heym, B., Allen, B., Young, D., and Cole, S. (1992) The catalase-peroxidase gene and isoniazid resistance of *Mycobacterium tuberculosis*. *Nature* **358,** 591–593

9. Rozwarski, D. A., Grant, G. A., Barton, D. H., Jacobs, W. R., Jr., and Sacchettini, J. C. (1998) Modification of the NADH of the isoniazid target (InhA) from *Mycobacterium tuberculosis. Science* **279,** 98–102
10. Guo, H., Seet, Q., Denkin, S., Parsons, L., and Zhang, Y. (2006) Molecular characterization of isoniazid-resistant clinical isolates of *Mycobacterium tuberculosis* from the U.S.A. *J. Med. Microbiol.* **55,** 1527–1531
11. Zhang, Y., Vilcheze, C., and Jacobs, W. R., Jr. (2005) in *Tuberculosis and the Tubercle Bacillus* (Cole, S. T., Eisenach, K. D., Jacobs, W. R., Jr., and McMurray, D. N., eds) 2nd Ed., pp. 115–140, American Society for Microbiology, Washington, D. C.
12. Suarez, J., Ranguelova, K., Schelvis, J. P., and Magliozzo, R. S. (2009) Antibiotic resistance in *Mycobacterium tuberculosis*: peroxidase intermediate bypass causes poor isoniazid activation by the S315G mutant of *M. tuberculosis* catalase-peroxidase (KatG). *J. Biol. Chem.* **284,** 16146–16155
13. Wiseman, B., Carpena, X., Feliz, M., Donald, L. J., Pons, M., Fita, I., and Loewen, P. C. (2010) Isonicotinic acid hydrazide conversion to isonicotinyl-NAD by catalase-peroxidases. *J. Biol. Chem.* **285,** 26662–26673
14. Cade, C. E., Dlouhy, A. C., Medzihradszky, K. F., Salas-Castillo, S. P., and Ghiladi, R. A. (2010) Isoniazid-resistance conferring mutations in *Mycobacterium tuberculosis* KatG: catalase, peroxidase, and INH-NADH adduct formation activities. *Protein Sci.* **19,** 458–474
15. Njuma, O. J., Ndontsa, E. N., and Goodwin, D. C. (2014) Catalase in peroxidase clothing: interdependent cooperation of two cofactors in the catalytic versatility of KatG. *Arch. Biochem. Biophys.* **544,** 27–39
16. Singh, R., Wiseman, B., Deemagarn, T., Jha, V., Switala, J., and Loewen, P. C. (2008) Comparative study of catalase-peroxidases (KatGs). *Arch. Biochem. Biophys.* **471,** 207–214
17. Moore, R. L., Powell, L. J., and Goodwin, D. C. (2008) The kinetic properties producing the perfunctory pH profiles of catalase-peroxidases. *Biochim. Biophys. Acta* **1784,** 900–907
18. Welinder, K. (1992) Superfamily of plant, fungal and bacterial peroxidases. *Curr. Opin. Struct. Biol.* **2,** 388–393
19. Zámocký, M., Furtmüller, P. G., and Obinger, C. (2010) Evolution of structure and function of Class I peroxidases. *Arch. Biochem. Biophys.* **500,** 45–57
20. Yamada, Y., Fujiwara, T., Sato, T., Igarashi, N., and Tanaka, N. (2002) The 2.0 angstrom crystal structure of catalase-peroxidase from *Haloarcula marismortui*. *Nat. Struct. Biol.* **9,** 691–695
21. Bertrand, T., Eady, N. A., Jones, J. N., Jesmin, Nagy, J. M., Jamart-Grégoire, B., Raven, E. L., and Brown, K. A. (2004) Crystal structure of *Mycobacterium tuberculosis* catalase-peroxidase. *J. Biol. Chem.* **279,** 38991–38999
22. Carpena, X., Loprasert, S., Mongkolsuk, S., Switala, J., Loewen, P. C., and Fita, I. (2003) Catalase-peroxidase KatG of *Burkholderia pseudomallei* at 1.7 A resolution. *J. Mol. Biol.* **327,** 475–489
23. Patterson, W. R., and Poulos, T. L. (1995) Crystal structure of recombinant pea cytosolic ascorbate peroxidase. *Biochemistry* **34,** 4331–4341
24. Finzel, B. C., Poulos, T. L., and Kraut, J. (1984) Crystal structure of yeast cytochrome *c* peroxidase refined at 1.7-A resolution. *J. Biol. Chem.* **259,** 13027–13036
25. Dunford, H. B. (1999) *Heme Peroxidases*, pp. 58–174, Wiley-VCH, New York
26. Zámocký, M., Regelsberger, G., Jakopitsch, C., and Obinger, C. (2001) The molecular peculiarities of catalase-peroxidases. *FEBS Lett.* **492,** 177–182
27. Kudalkar, S. N., Njuma, O. J., Li, Y., Muldowney, M., Fuanta, N. R., and Goodwin, D. C. (2015) A role for catalase-peroxidase large loop 2 revealed by deletion mutagenesis: control of active site water and ferric enzyme reactivity. *Biochemistry* **54,** 1648–1662
28. Jakopitsch, C., Droghetti, E., Schmuckenschlager, F., Furtmüller, P. G., Smulevich, G., and Obinger, C. (2005) Role of the main access channel of catalase-peroxidase in catalysis. *J. Biol. Chem.* **280,** 42411–42422
29. Kudalkar, S. N., Campbell, R. A., Li, Y., Varnado, C. L., Prescott, C., and Goodwin, D. C. (2012) Enhancing the peroxidatic activity of KatG by deletion mutagenesis. *J. Inorg. Biochem.* **116,** 106–115
30. Donald, L. J., Krokhin, O. V., Duckworth, H. W., Wiseman, B., Deemagarn, T., Singh, R., Switala, J., Carpena, X., Fita, I., and Loewen, P. C. (2003) Characterization of the catalase-peroxidase KatG from *Burkholderia pseudomallei* by mass spectrometry. *J. Biol. Chem.* **278,** 35687–35692
31. Jakopitsch, C., Kolarich, D., Petutschnig, G., Furtmüller, P. G., and Obinger, C. (2003) Distal side tryptophan, tyrosine and methionine in catalase-peroxidases are covalently linked in solution. *FEBS Lett.* **552,** 135–140
32. Ghiladi, R. A., Knudsen, G. M., Medzihradszky, K. F., and Ortiz de Montellano, P. R. (2005) The Met-Tyr-Trp cross-link in *Mycobacterium tuberculosis* catalase-peroxidase (KatG): autocatalytic formation and effect on enzyme catalysis and spectroscopic properties. *J. Biol. Chem.* **280,** 22651–22663
33. Ghiladi, R. A., Medzihradszky, K. F., and Ortiz de Montellano, P. R. (2005) Role of the Met-Tyr-Trp cross-link in *Mycobacterium tuberculosis* catalase-peroxidase (KatG) as revealed by KatG(M255I). *Biochemistry* **44,** 15093–15105
34. Jakopitsch, C., Auer, M., Ivancich, A., Rüker, F., Furtmüller, P. G., and Obinger, C. (2003) Total conversion of bifunctional catalase-peroxidase (KatG) to monofunctional peroxidase by exchange of a conserved distal side tyrosine. *J. Biol. Chem.* **278,** 20185–20191
35. Hillar, A., Peters, B., Pauls, R., Loboda, A., Zhang, H., Mauk, A. G., and Loewen, P. C. (2000) Modulation of the activities of catalase-peroxidase HPI of *Escherichia coli* by site-directed mutagenesis. *Biochemistry* **39,** 5868–5875
36. Regelsberger, G., Jakopitsch, C., Furtmüller, P. G., Rueker, F., Switala, J., Loewen, P. C., and Obinger, C. (2001) The role of distal tryptophan in the bifunctional activity of catalase-peroxidases. *Biochem. Soc. Trans.* **29,** 99–105
37. Yu, S., Girotto, S., Zhao, X., and Magliozzo, R. S. (2003) Rapid formation of Compound II and a tyrosyl radical in the Y229F mutant of *Mycobacterium tuberculosis* catalase-peroxidase disrupts catalase but not peroxidase function. *J. Biol. Chem.* **278,** 44121–44127
38. Suarez, J., Ranguelova, K., Jarzecki, A. A., Manzerova, J., Krymov, V., Zhao, X., Yu, S., Metlitsky, L., Gerfen, G. J., and Magliozzo, R. S. (2009) An oxyferrous heme/protein-based radical intermediate is catalytically competent in the catalase reaction of *Mycobacterium tuberculosis* catalase-peroxidase (KatG). *J. Biol. Chem.* **284,** 7017–7029
39. Zhao, X., Khajo, A., Jarrett, S., Suarez, J., Levitsky, Y., Burger, R. M., Jarzecki, A. A., and Magliozzo, R. S. (2012) Specific function of the Met-Tyr-Trp adduct radical and residues Arg-418 and Asp-137 in the atypical catalase reaction of catalase-peroxidase KatG. *J. Biol. Chem.* **287,** 37057–37065
40. Zhao, X., Suarez, J., Khajo, A., Yu, S., Metlitsky, L., and Magliozzo, R. S. (2010) A radical on the Met-Tyr-Trp modification required for catalase activity in catalase-peroxidase is established by isotopic labeling and site-directed mutagenesis. *J. Am. Chem. Soc.* **132,** 8268–8269
41. Zhao, X., Yu, S., Ranguelova, K., Suarez, J., Metlitsky, L., Schelvis, J. P., and Magliozzo, R. S. (2009) Role of the oxyferrous heme intermediate and distal side adduct radical in the catalase activity of *Mycobacterium tuberculosis* KatG revealed by the W107F mutant. *J. Biol. Chem.* **284,** 7030–7037
42. Jakopitsch, C., Vlasits, J., Wiseman, B., Loewen, P. C., and Obinger, C. (2007) Redox intermediates in the catalase cycle of catalase-peroxidases from *Synechocystis* PCC 6803, *Burkholderia pseudomallei*, and *Mycobacterium tuberculosis*. *Biochemistry* **46,** 1183–1193
43. Vlasits, J., Jakopitsch, C., Bernroitner, M., Zamocky, M., Furtmüller, P. G., and Obinger, C. (2010) Mechanisms of catalase activity of heme peroxidases. *Arch. Biochem. Biophys.* **500,** 74–81
44. Loewen, P. C., Carpena, X., Vidossich, P., Fita, I., and Rovira, C. (2014) An ionizable active-site tryptophan imparts catalase activity to a peroxidase core. *J. Am. Chem. Soc.* **136,** 7249–7252
45. Kruft, B. I., Magliozzo, R. S., and Jarzęcki, A. A. (2015) Density functional theory insights into the role of the methionine-tyrosine-tryptophan adduct radical in the KatG catalase Reaction: O_2 release from the oxyheme intermediate. *J. Phys. Chem. A* **119,** 6850–6866
46. Fita, I., Carpena, X., and Loewen, P. C. (2015) in *Heme Peroxidases* (Raven, E., and Dunford, B., eds) pp. 133–155, Royal Society of Chemistry, London
47. Gasselhuber, B., Jakopitsch, C., Zamocky, M., Furtmuller, P. G., and Obinger, C. (2015) in *Heme Peroxidases* (Raven, E., and Dunford, B., eds) pp. 156–180, Royal Society of Chemistry, London
48. Carpena, X., Wiseman, B., Deemagarn, T., Herguedas, B., Ivancich, A., Singh, R., Loewen, P. C., and Fita, I. (2006) Roles for Arg426 and Trp111 in

the modulation of NADH oxidase activity of the catalase-peroxidase KatG from *Burkholderia pseudomallei* inferred from pH-induced structural changes. *Biochemistry* **45,** 5171–5179

49. Carpena, X., Wiseman, B., Deemagarn, T., Singh, R., Switala, J., Ivancich, A., Fita, I., and Loewen, P. C. (2005) A molecular switch and electronic circuit modulate catalase activity in catalase-peroxidases. *EMBO Rep.* **6,** 1156–1162
50. Jakopitsch, C., Ivancich, A., Schmuckenschlager, F., Wanasinghe, A., Pöltl, G., Furtmüller, P. G., Rüker, F., and Obinger, C. (2004) Influence of the unusual covalent adduct on the kinetics and formation of radical intermediates in *Synechocystis* catalase peroxidase: a stopped-flow and EPR characterization of the Met275, Tyr249, and Arg439 variants. *J. Biol. Chem.* **279,** 46082–46095
51. Ghiladi, R. A., Medzihradszky, K. F., Rusnak, F. M., and Ortiz de Montellano, P. R. (2005) Correlation between isoniazid resistance and superoxide reactivity in *Mycobacterium tuberculosis* KatG. *J. Am. Chem. Soc.* **127,** 13428–13442
52. Gasselhuber, B., Graf, M. M., Jakopitsch, C., Zamocky, M., Nicolussi, A., Furtmüller, P. G., Oostenbrink, C., Carpena, X., and Obinger, C. (2016) Interaction with the redox cofactor MYW and functional role of a mobile arginine in eukaryotic catalase-peroxidase. *Biochemistry* **55,** 3528–3541
53. Vidossich, P., Alfonso-Prieto, M., Carpena, X., Loewen, P. C., Fita, I., and Rovira, C. (2007) Versatility of the electronic structure of compound I in catalase-peroxidases. *J. Am. Chem. Soc.* **129,** 13436–13446
54. Claiborne, A., and Fridovich, I. (1979) Purification of the *o*-dianisidine peroxidase from *Escherichia coli* B. Physicochemical characterization and analysis of its dual catalatic and peroxidatic activities. *J. Biol. Chem.* **254,** 4245–4252
55. Ndontsa, E. N., Moore, R. L., and Goodwin, D. C. (2012) Stimulation of KatG catalase activity by peroxidatic electron donors. *Arch. Biochem. Biophys.* **525,** 215–222
56. Singh, R., Switala, J., Loewen, P. C., and Ivancich, A. (2007) Two [Fe(IV)=O Trp^{+}] intermediates in *M. tuberculosis* catalase-peroxidase discriminated by multifrequency (9–285 GHz) EPR spectroscopy: reactivity toward isoniazid. *J. Am. Chem. Soc.* **129,** 15954–15963
57. Colin, J., Wiseman, B., Switala, J., Loewen, P. C., and Ivancich, A. (2009) Distinct role of specific tryptophans in facilitating electron transfer or as [Fe(IV)=O Trp(*)] intermediates in the peroxidase reaction of *Bulkholderia pseudomallei* catalase-peroxidase: a multifrequency EPR spectroscopy investigation. *J. Am. Chem. Soc.* **131,** 8557–8563
58. Ivancich, A., Dorlet, P., Goodin, D. B., and Un, S. (2001) Multifrequency high-field EPR study of the tryptophanyl and tyrosyl radical intermediates in wild-type and the W191G mutant of cytochrome *c* peroxidase. *J. Am. Chem. Soc.* **123,** 5050–5058
59. Sivaraja, M., Goodin, D. B., Smith, M., and Hoffman, B. M. (1989) Identification by ENDOR of Trp191 as the free-radical site in cytochrome-*c* peroxidase compound ES. *Science* **245,** 738–740
60. Wiseman, B., Colin, J., Smith, A. T., Ivancich, A., and Loewen, P. C. (2009) Mechanistic insight into the initiation step of the reaction of *Burkholderia pseudomallei* catalase-peroxidase with peroxyacetic acid. *J. Biol. Inorg. Chem.* **14,** 801–811
61. Ivancich, A., Donald, L. J., Villanueva, J., Wiseman, B., Fita, I., and Loewen, P. C. (2013) Spectroscopic and kinetic investigation of the reactions of peroxyacetic acid with *Burkholderia pseudomallei* catalase-peroxidase, KatG. *Biochemistry* **52,** 7271–7282
62. Yu, S., Chouchane, S., and Magliozzo, R. S. (2002) Characterization of the W321F mutant of *Mycobacterium tuberculosis* catalase-peroxidase KatG. *Protein Sci.* **11,** 58–64
63. Gray, H. B., and Winkler, J. R. (2015) Hole hopping through tyrosine/tryptophan chains protects proteins from oxidative damage. *Proc. Natl. Acad. Sci. U.S.A.* **112,** 10920–10925
64. Yukl, E. T., Williamson, H. R., Higgins, L., Davidson, V. L., and Wilmot, C. M. (2013) Oxidative damage in MauG: implications for the control of high-valent iron species and radical propagation pathways. *Biochemistry* **52,** 9447–9455
65. Kathiresan, M., and English, A. M. (2017) LC-MS/MS suggests that hole hopping in cytochrome c peroxidase protects its heme from oxidative modification by excess H_2O_2. *Chem. Sci.* **8,** 1152–1162
66. Jakopitsch, C., Obinger, C., Un, S., and Ivancich, A. (2006) Identification of Trp106 as the tryptophanyl radical intermediate in *Synechocystis* PCC6803 catalase-peroxidase by multifrequency electron paramagnetic resonance spectroscopy. *J. Inorg. Biochem.* **100,** 1091–1099
67. Ranguelova, K., Suarez, J., Magliozzo, R. S., and Mason, R. P. (2008) Spin trapping investigation of peroxide- and isoniazid-induced radicals in *Mycobacterium tuberculosis* catalase-peroxidase. *Biochemistry* **47,** 11377–11385
68. Zhao, X., Girotto, S., Yu, S., and Magliozzo, R. S. (2004) Evidence for radical formation at Tyr-353 in *Mycobacterium tuberculosis* catalase-peroxidase (KatG). *J. Biol. Chem.* **279,** 7606–7612
69. Moore, S. (October 2016) 'Round-the-horn site-directed mutagenesis-OpenWetWare in http://openwetware.org/wiki/'Round-the-horn_site-directed_mutagenesis (Please note that the JBC is not responsible for the long-term archiving and maintenance of this site or any other third party hosted site.)
70. Varnado, C. L., and Goodwin, D. C. (2004) System for the expression of recombinant hemoproteins in *Escherichia coli*. *Protein Expr. Purif.* **35,** 76–83
71. Falk, J. K. (1964) in *Porphyrins and Metalloporphyrins* (Smith, K. M., ed) pp. 804–807, Elsevier Publishing, New York
72. Scott, S. L., Chen, W. J., Bakac, A., and Espenson, J. H. (1993) Spectroscopic parameters, electrode-potentials, acid ionization-constants, and electron-exchange rates of the 2,2′-azinobis(3-ethylbenzothiazoline-6-sulfonate) radicals and ions. *J. Phys. Chem.* **97,** 6710–6714
73. Nelson, D. P., and Kiesow, L. A. (1972) Enthalpy of decomposition of hydrogen-peroxide by catalase at 25 degrees C (with molar extinction coefficients of H_2O_2 solutions in UV). *Anal. Biochem.* **49,** 474–478
74. Goodwin, D. C., Yamazaki, I., Aust, S. D., and Grover, T. A. (1995) Determination of rate constants for rapid peroxidase reactions. *Anal. Biochem.* **231,** 333–338
75. Goodwin, D. C., and Hertwig, K. M. (2003) Peroxidase-catalyzed oxidation of capsaicinoids: steady-state and transient-state kinetic studies. *Arch. Biochem. Biophys.* **417,** 18–26
76. Liu, A., Pötsch, S., Davydov, A., Barra, A. L., Rubin, H., and Gräslund, A. (1998) The tyrosyl free radical of recombinant ribonucleotide reductase from *Mycobacterium tuberculosis* is located in a rigid hydrophobic pocket. *Biochemistry* **37,** 16369–16377
77. DeLano, W. L. (2013) *The MacPyMOL Molecular Graphics System*, version 1.6.0.0, Schrodinger, LLC, New York
78. Zhao, X., Yu, H., Yu, S., Wang, F., Sacchettini, J. C., and Magliozzo, R. S. (2006) Hydrogen peroxide-mediated isoniazid activation catalyzed by *Mycobacterium tuberculosis* catalase-peroxidase (KatG) and its S315T mutant. *Biochemistry* **45,** 4131–4140